INTERFACE
FOCUS

rsfs.royalsocietypublishing.org

Research

Cite this article: Zhu J, Mogilner A. 2016 Comparison of cell migration mechanical strategies in three-dimensional matrices: a computational study. *Interface Focus* **6**: 20160040.
http://dx.doi.org/10.1098/rsfs.2016.0040

One contribution of 12 to a theme issue 'Coupling geometric partial differential equations with physics for cell morphology, motility and pattern formation'.

Subject Areas:
biomathematics, biophysics, computational biology

Keywords:
cell migration, three-dimensional, computational model, cell mechanics

Author for correspondence:
Alex Mogilner
e-mail: mogilner@cims.nyu.edu

Electronic supplementary material is available at http://dx.doi.org/10.1098/rsfs.2016.0040 or via http://rsfs.royalsocietypublishing.org.

THE ROYAL SOCIETY
PUBLISHING

Comparison of cell migration mechanical strategies in three-dimensional matrices: a computational study

Jie Zhu[1] and Alex Mogilner[2]

[1]Nanobiology Institute and Department of Cell Biology, Yale University, New Haven, CT, USA
[2]Courant Institute and Department of Biology, New York University, New York, NY, USA

AM, 0000-0001-5302-2404

Cell migration on a two-dimensional flat surface has been extensively studied and is generally characterized by a front-protrusion–rear-contraction process. In a three-dimensional (3D) environment, on the other hand, cells adopt multiple migration strategies depending on the cell type and the properties of the extracellular matrix (ECM). By using computer simulations, we find that these migration strategies can be classified by various spatial–temporal dynamics of actin protrusion, actin–myosin contraction and actin–ECM adhesion. We demonstrate that if we include or exclude proteolysis of ECM, and vary adhesion dynamics and spatial distributions of protrusion, contraction and adhesion, our model can reproduce six experimentally observed motility modes: mesenchymal, chimneying, amoeboid, blebbing, finger-like protrusion and rear-squeezing cell locomotory behaviours. We further find that the mode of the cell motility evolves in response to the ECM density and adhesion detachment rate. The model makes non-trivial predictions about cell speed as a function of the adhesion strength, and ECM elasticity and mesh size.

1. Introduction

Actin-based cell migration is a key process for morphogenesis, wound healing and cancer invasion [1]. Cell migration has been extensively studied on two-dimensional (2D) substrates. It typically involves a combination of front protrusion, rear contraction and graded adhesion [1]. At the leading edge, actin polymerization forms flat and wide protruding lamellipodia [2]. At the rear, myosin-induced contraction and disassembly of the actin networks generate contraction and forward translocation of the cell body [2]. Dynamic adhesions [3,4] are formed in the lamellipodia region, mature and disassemble as they move towards the centre of the cell [5]. The migration speed of cells is determined by a delicate balance among actin polymerization, myosin-powered retrograde actin flow, and an effective adhesion drag [6].

In a more physiologically relevant three-dimensional (3D) environment, however, cell migration is far less understood due to both the technical challenges and the complexity of migratory behaviours. For example, fibroblasts are found to move through 3D matrices in either lobopodial or lamellipodial mode [7]. The former was observed in a stiff extracellular matrix (ECM) where fibroblasts have an elongated shape and translocate using blunt, cylindrical protrusions. The latter was observed in a soft collagen matrix or at low RhoA activity where fibroblasts form branched, finger-like pseudopodia with Rac1 and Cdc42 activated at the tips. Both lobopodial and lamellipodial modes require integrin-based adhesions, as inhibition of integrin stops the motion of the cells [7]. Cell migration in ECM normally depends on myosin-based contraction within the pseudopodia [8] that is several micrometres behind the tips of pseudopodia [9]. In the fibroblasts migrating in the ECM [7], nuclei are located at the centre or rear of the cells; however, migrating epithelial cells in 3D collagen matrices were observed to have their nuclei leading the cell front with contractile cell body trailing behind [10] and with actomyosin contraction propelling the nuclei forward and driving the migration of these cells.

Tumour cells often migrate in either mesenchymal or amoeboid mode, depending on both the cellular properties and the physical properties of the ECM [11]. In mesenchymal mode, cells are polarized and have an elongated shape, with protrusion and retraction located at the two opposite ends and integrin-dependent adhesions distributed all over the cell surface. Cells exert traction forces on the ECM and translocate with a continuous release of adhesions at the rear. Mesenchymal migration relies on proteolytic activity to melt down the ECM barriers and reduce the resistance [12]. Such migration causes structural remodelling of the ECM as the cells advance through the ECM. In amoeboid mode, cells are less polarized and have a more rounded shape. They have a more uniform distribution of cortical actin and form either F-actin networks or membrane blebs in the direction of migration [7,11]. Cells in amoeboid mode migrate by squeezing through the pores of the ECM without remodelling it. Both the proteolytic activity and the adhesion level are minimal in amoeboid mode [6].

Perturbations of both internal and external factors have shed light on multiple aspects of mechanochemistry of cell migration in 3D. Inhibition of proteolytic activity in tumour cells causes them to switch from mesenchymal to amoeboid mode, while recovery of proteolytic activity brings the cells back to the mesenchymal mode [11]. This indicates the existence of multiple, either complementary or redundant, mechanisms in cell migration. Recent study showed that mesenchymal migration depends on Rac-activated protrusion of actin, and that amoeboid migration relies on Rho-activated myosin contractility [13]. Because of complex feedbacks between Rac and Rho, the balance between these two GTPases is likely to determine the migration strategy of tumour cells. Modes of cell migration also depend on the stiffness of the ECM. It has been shown that decreasing the stiffness of the matrix causes migrating fibroblasts to switch from lobopodial mode to lamellipodial mode, and that restoring the stiffness recovered the migration to lobopodial mode [7]. The pore size of the matrix also influences the migration mode. Tumour cells lacking proteolysis can move in amoeboid mode in collagen matrix, but not so in a denser Matrigel matrix [14]. On the other hand, fibroblasts in a sparse matrix were found to migrate along individual fibres in a peculiar one-dimensional fashion [15,16].

Despite these intriguing findings, quantitative understanding of the dynamics of key molecular processes and mechanics of 3D migration remains elusive. Computational modelling is a valuable complement to experiments in understanding the complex cell migration behaviours [16]. Early computational models did not address the shape change of the cells but focused on factors that influence the speed of migration. Zaman *et al.* [17] proposed a force balance model with prescribed force profile and adhesion dynamics. They predicted that the speed of cell has a similar biphasic dependence on the cell–matrix adhesion to cells moving on a 2D surface. Borau *et al.* [18] developed a continuum approach to investigate how the stiffness of the ECM influences the cell migration. Each modelled cell in their model is simplified as a self-protrusive 3D elastic unit that interacts with an elastic substrate through detachable bonds. They found a biphasic dependence of cell speed on substrate stiffness: cell speed is highest with an optimal ECM stiffness; increasing or decreasing the stiffness leads to a lower cell speed. Recent models place more emphasis on both the shape of migrating cells and the dynamics of actin networks in cells. Hawkins *et al.* [19] analysed the instability of the actomyosin cortex on a spherical surface and showed that cell migration can be induced by an emerging flow of the actin cortex driven by the accumulation of myosin at one of the cell poles, and subsequent pulling of the actin network towards this pole maintaining higher myosin concentration there. Friction between this flow and ECM has been proposed to propel the cell. Sakamoto *et al.* [20] proposed a computational model that takes into account the viscoelastic property of the cell body. The model incorporates the shape change of the cell by using a finite-element method. With a prescribed cyclic protrusion of the leading edge of the cell, the authors predicted that the mesenchymal-to-amoeboid transition is caused by a reduced adhesion and an increased switching frequency between protrusion and contraction. The most prominent recent modelling success is the study of Tozluoglu *et al.* [21] which reported a detailed, agent-based model of blebbing driving amoeboid migration of cancer cells. The cell cortex and membrane, represented by a series viscoelastic links, encompass a viscoelastic interior of the cell. By comparing cell migration through a smooth chamber and discrete grids, the authors predicted that adhesion levels affect the migration speed, and that steric interaction between the cells and the ECM provides traction forces for amoeboid mode of migration.

Most of the above models focused on one migration mode and did not address the transition or relation between different migration modes. Here we present an agent-based model that includes both the dynamics of the cytoskeleton inside the cell and the physical interactions between the cell and the structure of the ECM. The model also accounts for the dynamic shape change of the cell. By varying the actin–myosin dynamics and cell–ECM interactions, we are able to reproduce various observed 3D migration modes. We demonstrate computationally that spatially separated protrusion and the contraction of the cytoskeleton are essential for cell migration in 3D, and that the steady flow of actin is the main driving force for cell migration. Adhesion to the ECM, however, is dispensable if steric interactions between the cell and the ECM are strong. We also predict which migration strategy optimizes cell migration based on the physical properties of the ECM and the cell–ECM interactions.

2. Computational model

To avoid great computational complexity of true 3D simulations, we consider a planar cross section of the cell and a cross section of the ECM in the same plane around the cell. This planar section of the cell has anterior–posterior and dorsal–ventral directions but not lateral sides. One mathematical way to think about the model is to imagine a cylindrical cell extending a great distance from side to side and both the cell and the ECM are homogeneous in that direction so that all non-trivial effect occurs in the 2D cross-sectional plane. Another, also mathematical, approximation is to consider an axially symmetric cell embedded into an axially symmetric ECM, and to neglect geometric effects of the polar coordinate system on the mechanics and transport.

More realistically though, the model is really 2D, but it captures most essential 3D migration effects: squeezing of the deformable and 'active' cell through the deformable ECM.

The simulated cell consists of a dynamic actin–myosin network, a rigid nucleus, and an elastic membrane (figure 1). The cell is embedded into an ECM represented by a 2D node-spring network in the x–y plane. The migrating virtual cell has physical interactions with the nodes of the ECM. ECM in the model is treated as a 2D elastic spring-node network. The actin–myosin network of the cell is also represented by a 2D node-spring network, similar to previous works [22–24]. Each node in this network connects to up to six nearby neighbouring nodes through linear springs with a finite rest length and a spring constant k_s, which contributes to the elastic stiffness of the network. The angular stiffness of the springs is not included because the structure of the connection gives rise to shear resistance [22]. We focus on directed cell migration and thus ignore the initial process of symmetry breaking. The simulated cell is assumed to have a fixed direction of polarization, which corresponds, for example, to cell migration in a fixed gradient of chemoattractant.

To incorporate the protrusion and contraction behaviour of the actin–myosin network, we model the network in the following way. At the front of the cell, the nucleation of the new actin filaments is incorporated by adding new nodes to the existing network along the leading edge at an overall nucleation rate k_{nuc}. Each new node is immediately incorporated into the existing network by connecting to six neighbouring nodes with undeformed springs. The initial rest length of each spring is the same as the initial distance between the connected nodes. The polymerization and expansion of the network is represented by the continuous elongation of the rest lengths of springs with a speed v_g until the rest lengths reach a maximum value $l_{\max} = 0.8R_{\mathrm{nuc}} = 4\,\mu\mathrm{m}$, where R_{nuc} is the radius of the nucleus and is a natural length scale in the model. As the network expands, it creates an expansive stress in all directions. Such expansion of the actin network is restricted to the front half of the cell to represent the protrusion of actin at the front. At the rear of the cell, the actin network undergoes myosin-induced contraction which is approximated by the continuous shortening of the rest lengths of springs with speed v_s. The shortening of the springs creates a contractile stress in the network. Such activity is restricted to the rear half of the cell. To include the effect of the network disassembly, each network node is removed when its lifetime reaches $1/k_{\mathrm{dis}}$, where k_{dis} is the disassembly rate. The nucleus is treated as a hard sphere inside the cell which has steric interactions with both the actin–myosin network and the cell membrane (nodes of neither network nor membrane penetrate the nucleus). Note that many biophysical processes—growth and disassembly of a few types of actin structures, hydrostatic/osmotic pressure, dynamic cross-linking, myosin contraction—can contribute in complex ways to the net rates and forces of expansion and contraction; our coarse-grained model does not address these microscopic mechanisms.

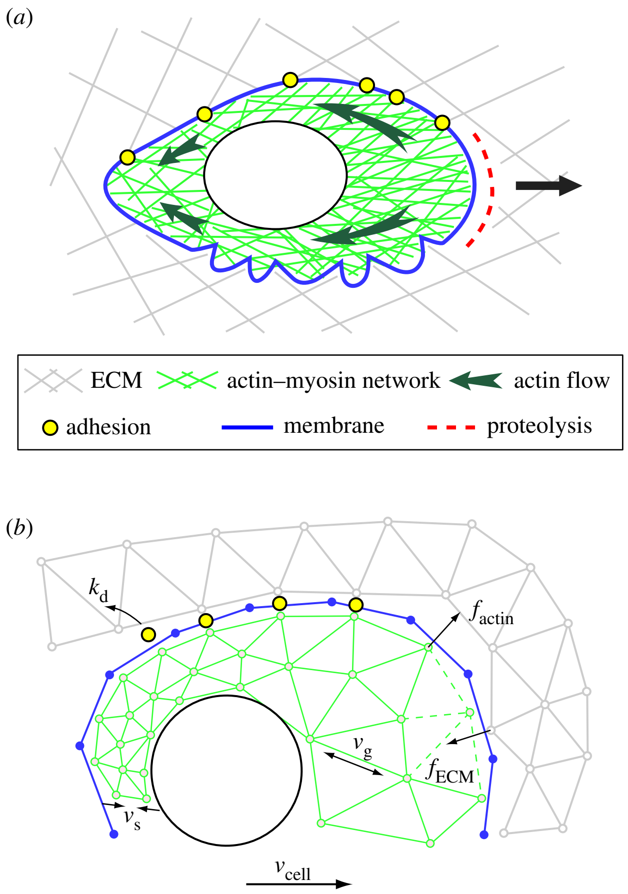

Figure 1. Schematics of the model. Actin–myosin network is shown in green; ECM network is shown in grey; nucleus is shown as white disc; cell membrane is shown in blue; adhesions are yellow circles. Cell membrane and actin–myosin and ECM networks are node-and-spring networks. (*a*) Conceptual model. Cell can interact with ECM via both adhesions (upper membrane surface) and steric effects (lower membrane surface). (*b*) Node-spring networks in the simulation. The actin–myosin network links undergoing spatially graded expansion with rate v_g and contraction with rate v_s, respectively. Effective elastic force from the outer nodes of this network, f_{actin}, acts on the membrane; similarly, effective elastic force, f_{ECM}, from the ECM nodes that are pressing on the membrane or adhering to it is ultimately transduced to the cell. The adhesions detach with rate k_d.

The cell membrane is represented by a node-spring chain, which separates the actin network from the ECM. The initial perimeter of the membrane for a disc-like cell is chosen to be $L = 2\pi R_{\mathrm{cell}} \approx 50\,\mu\mathrm{m}$. The total number of membrane nodes is 50 in the simulations so that the rest length of each membrane segment is $\Delta L = L/50 \approx 1\,\mu\mathrm{m}$. The stretching spring constant for each membrane link is assumed to be $k_{\mathrm{s,mem}} = 500\ \mathrm{pN}\,\mu\mathrm{m}^{-1}$ and the bending rigidity is chosen to be $k_{\mathrm{b,mem}} = 10\ \mathrm{pN}\,\mu\mathrm{m}$ per link-pair. This bending rigidity is arbitrarily chosen to avoid membrane crossing. In reality, such bending rigidity may also come from the actin cortex that is attached to the cell membrane. To further avoid the self-crossing of the simulated membrane, we included a Gaussian-shaped repulsive energy between the membrane nodes. The repulsive energy on each membrane node has a maximum range of one segment length so that it has effect only if two membrane nodes are closer than the segment length. The membrane interacts with both the actin–myosin network and the ECM nodes through steric effects. The motion of each membrane node is determined by the force through Stokes' law.

Outside the cell, the ECM is modelled as a 2D node-spring triangular network with an average mesh size of $\xi_{\mathrm{ECM}} = 10\,\mu\mathrm{m}$. We assume that the ECM in our 2D simulation represents a layer of 3D ECM with the same mesh size. Thus, the spring constant of the ECM links is $k_s = Y_{\mathrm{ECM}}\xi_{\mathrm{ECM}}$, where

Table 1. Definition and values of parameters.

symbols	definition	values
ξ_{ECM}	mesh size of ECM	2–10 μm
R_{cell}	effective cell radius	6–8 μm
R_{nuc}	radius of nucleus	5 μm
k_{nuc}	nucleation rate of actin nodes	$1\ \mathrm{s}^{-1}$
k_{dis}	disassembly rate constant of actin nodes	$0.004\ \mathrm{s}^{-1}$
k_{d}	detachment rate constant of adhesion sites	$0.02\ \mathrm{s}^{-1}$
k_{n}	formation rate of adhesion sites	$0.05\ \mathrm{s}^{-1}$
v_{g}	growth speed of actin links	$0.01\ \mu\mathrm{m\ s}^{-1}$
v_{s}	shrinking speed of actin links	$0.002\ \mu\mathrm{m\ s}^{-1}$
Y_{ECM}	Young's modulus of ECM	10 Pa
$k_{\mathrm{s,ctx}}$	spring constant of actin link	$1000\ \mathrm{pN}\ \mu\mathrm{m}^{-1}$
$k_{\mathrm{s,mem}}$	spring constant of membrane link	$500\ \mathrm{pN}\ \mu\mathrm{m}^{-1}$
$k_{\mathrm{b,mem}}$	bending stiffness for membrane link	$10k_{\mathrm{B}}\,T$

Y_{ECM} is the Young's modulus of the ECM. To include the rupture of the ECM, we assume that each spring in the ECM breaks when it is stretched beyond a critical force f_{c}. For ECM of the same component and structure, parameter f_{c} is likely to be proportional to the thickness of the fibres in the matrix and is thus proportional to the stiffness the ECM. Therefore, we assume f_{c} to be proportional to Y_{ECM} via $f_{\mathrm{c}} = 100Y_{\mathrm{ECM}}\ \mathrm{pN\,Pa}^{-1}$. For ECM with $Y_{\mathrm{ECM}} = 10\,\mathrm{Pa}$, the critical force is $f_{\mathrm{c}} = 1000$ pN.

We assume that cells interact only with the nodes of ECM, and that the springs between the ECM nodes only provide restoring forces to the nodes. We include both the steric interaction and transient adhesions between the cell and the ECM nodes. New adhesions are formed when the distance between the actin nodes and the ECM nodes is within half of the average mesh size of the actin network of approximately 0.4 μm. Each adhesion site joins the two nodes together until the adhesion detaches, which has a rate constant of $k_{\mathrm{d}} = 0.02\,\mathrm{s}^{-1}$.

To include the proteolysis into the model, we assume that the proteolytic activity is restricted to the leading edge of the cell with a width of half the diameter of the cell, approximately 0.4 μm. If an ECM node is in contact with the proteolytic region, both the ECM node and its connected springs are removed from the ECM without a time delay.

We have also included an effective pressure to account for the approximate conservation of cell area: $\Delta P = \alpha(1 - A/A_0)$, where $\alpha = 1\ \mathrm{pN}\ \mu\mathrm{m}^{-2}$ is an arbitrary constant to preserve the area, A is the current area of the cell and A_0 is the initial area of the cell. The force produced by this pressure on each membrane node is $f_{\mathrm{i}} = \xi_{\mathrm{mem}}\Delta P$ along the outward normal.

3. Simulation procedure

The simulated cell initially has a circular shape with radius $R_{\mathrm{cell}} = 6$–8 μm (figure 1; tables 1 and 2). A circular nucleus of $R_{\mathrm{nuc}} = 5$ μm is at the centre of the cell. The cell is placed in a 60 × 120 μm rectangular strip of ECM and has a fixed migration direction along the x-direction. The ECM is fixed along the wall of the chamber with an average pore size of 2–10 μm.

At the beginning of each simulation, the ECM is undeformed such that all the links are at their rest lengths. A cell is placed at the left end of the ECM and has a fixed direction of polarity towards the right. When the cell is placed inside the ECM, it deforms the ECM by steric interactions. Since both the cell and the ECM are in force balance during the migration, equal but opposite forces are applied to the ECM and the cell. ECM nodes move to the position of force equilibrium. The cell experiences opposite forces and undergoes deformation in a similar fashion.

At each time step Δt in the simulations, all the springs in the actin network are relaxed to reach force equilibrium. To model the nucleation of new filaments, a total of $k_{\mathrm{nuc}}\Delta t$ new cytoskeletal nodes are added randomly along the leading edge of the cell and immediately connected to nearby existing nodes with undeformed linear springs. To model the disassembly of the actin network of N nodes, a total of $k_{\mathrm{dis}}N\Delta t$ existing cytoskeletal nodes, together with their connected springs, are randomly removed from the simulation at each time interval Δt. The rest lengths of links at the front half of the cell elongate at a constant rate before reaching a maximum value of $l_{\max}$ to represent the polymerization of the actin networks: $\Delta l_{\mathrm{i}} = v_{\mathrm{g}}\Delta t$. The rest lengths of springs at the rear half of the cell shorten at a constant rate to represent the contraction of the actin networks: $\Delta l_{\mathrm{i}} = -v_{\mathrm{s}}\Delta t$. The adhesion between the cell and the ECM is represented by connecting the cytoskeletal nodes and their adjacent ECM nodes. The lifetime of each adhesion is calculated as $\tau = 1/k_{\mathrm{d}}$.

We find that the cytosol-caused viscous drag on the actin network is negligible compared with the internal elastic stress in the network. Therefore, the motion of the nodes of actin network is determined by the force balance of the elastic springs, and the cytoskeletal nodes always move to their force-equilibrium positions. The force on each node is the sum of the forces from the connected springs: $\boldsymbol{F} = \sum_i \boldsymbol{f}_i$. The force equilibrium for each node with n links is approximated as $\boldsymbol{F}/nk_{\mathrm{s}}$ from the current position and is then further adjusted according to energy minimization.

Nodes in both the actin–myosin network and ECM interact with membrane segments through steric interactions. The movement of each node on the membrane is approximated by $F/2k_{\mathrm{s}}$ towards the equilibrium position. The motion satisfies the condition that each individual node in the actin network, membrane and ECM reaches force equilibrium. As a result, the net forces on the actin network, cell membrane and the ECM are all zero.

Each round of the simulation ends when the cell moves close to the right end of the ECM or the total simulated time reaches 3 hours of real time. The average speed of the cell for each run is calculated by dividing the travelled distance of the nucleus by the total simulated time. Each set of parameters are simulated for 100 times to obtain the average migration speed of the cell.

The baseline model parameters (some of which vary in the simulations described below) are gathered in table 1. Parameters ξ_{ECM}, R_{cell} and R_{nuc} are of the same order of magnitude as those reported in [11]. Parameter Y_{ECM} is of the same order of magnitude as that reported in [14].

Table 2. Parameters for different migration modes.

	amoeboid	chimneying	finger-like	mesenchymal	rear-squeezing
proteolysis	n	y	n	y	y
adhesion	y/n	n	y	y	y
ξ_{ECM} (μm)	10	5	2	2	2
R_{cell} (μm)	8	8	6	8	6

The adhesion detachment rate is chosen to correspond to the effective adhesion level investigated in [14]. The rates of adhesion formation, network nucleation, assembly, disassembly, growth, shrinking and spring constants are chosen so that the network flow and deformations similar to those widely reported in the experimental literature are reproduced.

4. Results

4.1. Migration modes depend on the distribution and dynamics of protrusion, contraction and adhesion as well as extracellular matrix properties

By altering the spatial distribution and dynamics of actin protrusion, actin–myosin contraction and adhesion in our simulations (figures 2 and 3; table 2), we find six migration modes similar to those observed in normal and tumour cells. Three of those are shown in electronic supplementary material, Movies S1–S3 (table 3).

4.1.1. Mesenchymal mode

This mode is common in cancer cells with strong proteolytic activity and adhesions. When proteolytic activity is included and low-adhesion detachment rate of $k_{\mathrm{d}} = 0.02\,\mathrm{s}^{-1}$ is chosen, the simulated cell shows an elongated shape with nucleus located at the rear (figures 2*a* and 3*a*; electronic supplementary material, Movie S1), consistent with the observed shape of mesenchymal cells. The front end is pushed by the polymerization and expansion of the actin networks, while the rear end is retracted by the adhesion sites between the cell and the ECM. Proteolytic activity is crucial for this mode, as it removes the hindering ECM nodes at the front and facilitates efficient migration.

Cells migrating in mesenchymal mode form transient adhesion bonds between the moving actin network and the outside ECM throughout the side of the cell. At the front of the cell, adhesions provide traction forces because the local flow rate of actin network is faster than cell translocation rate v_{cell}. As adhesion sites move towards the rear of the cell, the local flow speed of the actin network decreases. When the local flow speed of actin becomes slower than v_{cell}, the adhesions generate resistant forces on the cell. Since the adhesions gradually mature and detach from the cell as they move towards the rear, the cells are able to move forward continuously.

4.1.2. Chimneying mode

Our simulations show that inhibition of adhesion does not totally stop the motion of the mesenchymal cells. Cells with proteolytic activity can move in a dense ECM using a chimneying mode (named by analogy with model [25]) where small protrusions form and extend into the ECM pores on the side of the cells (figures 2*b* and 3*a*; electronic supplementary material, Movie S2). Since these protrusions contain actin networks that are integral and mechanically connected parts of the whole actin network, the retrograde flow of actin in the cell generates traction forces via steric effect between the protrusions and the ECM. Cells' movement in this mode is less efficient compared with those moving in mesenchymal mode because of the low efficiency in the generation of traction forces.

4.1.3. Amoeboid and blebbing modes

This mode of migration emerges when proteolysis is inhibited and the adhesion level is low. We have simulated this migration mode by turning off the proteolytic activity. With a low detachment rate of $k_{\mathrm{d}} = 0.02\,\mathrm{s}^{-1}$, the simulated cell keeps forming random pseudopodia-like protrusions into adjacent pores of the ECM (figure 2*c*; electronic supplementary material, Movies S3 and S4). Because actin polymerization keeps expanding at the front, the protrusions inside the ECM pores keep growing in size. Eventually, one protrusion will dominate and pulls the rest of the cell into that direction due to the conservation of cell volume. This mode of migration is similar to the observed amoeboid mode of migration.

By completely removing the formation of adhesion sites, we find the simulated cell has a similar motion except that the adhesion-based cell–ECM interactions have been replaced by steric effects (figures 2*d* and 3*b*). Cell moving in this mode has a lower speed due to the less effective generation of traction forces. This mode is similar to the observed blebbing mode [26,27]. We emphasize that the experimentally observed blebbing mode has been well explained by the detachment of the membrane from the actin cortex and subsequent pushing by the hydrostatic pressure. Our model does not simulate the experimentally observed mechanism; we simply note that our model generates the morphodynamic behaviour similar to that of the blebbing mode.

4.1.4. Finger-like protrusion mode

It has been shown that cells can migrate by forming long, finger-like protrusions from the cell body into the ECM and generates traction forces from the tips of the protrusions [9]. We hypothesize that such a shape can be reproduced by our model (figures 2*e* and 3*c*; electronic supplementary material, Movie S5) if both the actin polymerization and the adhesion formation are active inside the protrusion. We

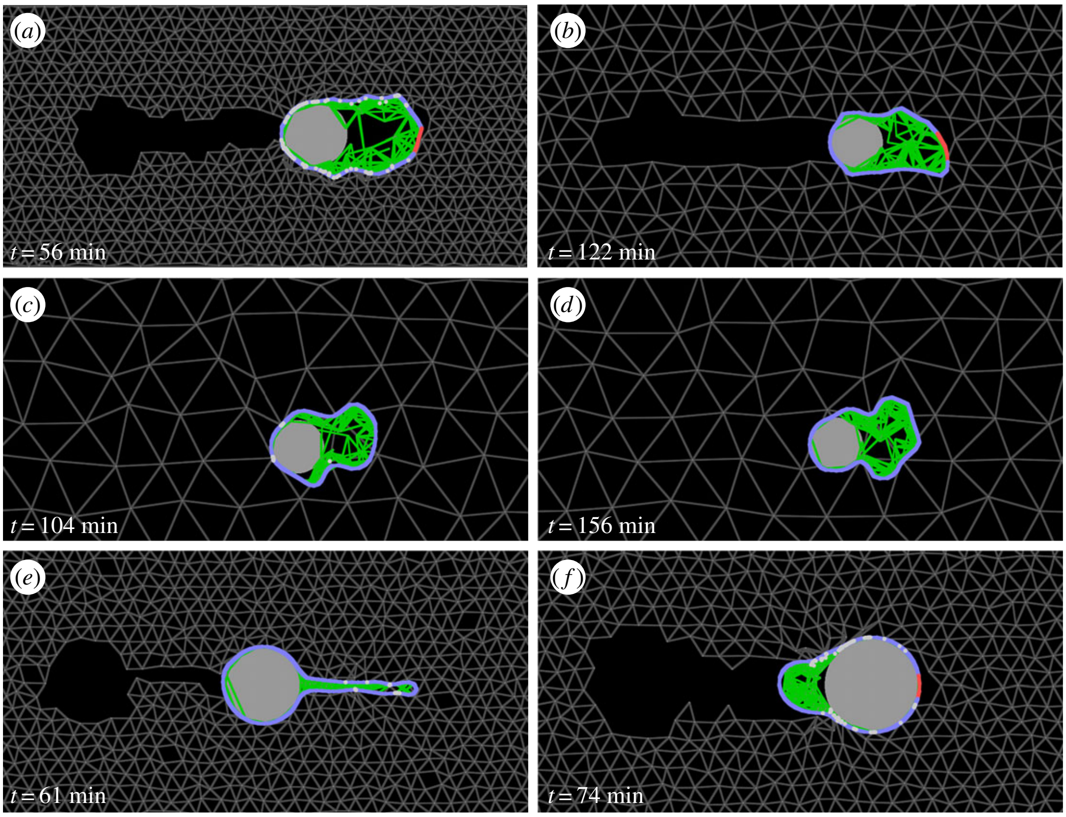

Figure 2. Simulation snapshots. (*a*) Mesenchymal mode, (*b*) chimneying mode, (*c*) amoeboid mode, (*d*) blebbing mode, (*e*) finger-like mode and (*f*) rear-squeezing mode. In all figures, actin network is shown in green; nuclei are shown as grey circles; cell membrane is shown in blue; ECM is shown as grey triangular meshwork outside the cell; proteolytic region is shown in red; and cell–ECM adhesion sites are shown as white dots on the membrane.

have also changed the cell radius to 6 μm to reduce the size of the simulated protrusion (12 μm long and 2 μm wide). With a strong myosin-mediated contraction, the simulated actin network exerts a high contraction force between the protrusion and the rest of the cell body. Because the protrusion has a high concentration of adhesion sites, the cell body is pulled along the protrusion. At the tip of the protrusion, actin polymerization pushes the cell membrane further into the pores of the ECM against the local adhesions, allowing a continuous migration of the cell.

This mode of migration requires rupture of ECM links in the neck region of the migrating cell. Although local proteolysis of ECM can greatly enhance such effect, we find that proteolysis is dispensable. Without proteolysis, our simulated cell can keep moving if (i) the contractile force in the protrusion is strong, (ii) the adhesions are strong and evenly distributed along the protrusion and (iii) the ECM is easy to rupture.

4.1.5. Rear-squeezing mode

To mimic the nucleus-at-front migration type observed in [10], we reduced the radius of simulated cell to 6 μm so that the nucleus occupies a higher fraction of the cell volume. In addition, we make 90% of the actin nucleation events at the rear half of the cell. As a result, most of the actin network is concentrated behind the nucleus, and the contraction of the actin network is able to generate a squeezing force on the nucleus to push the cell forward (figure 2*f*). Cell–ECM adhesion is required in this migration mode, as steric interactions between the cell and the ECM are greatly reduced due to the small contact region between the rear of the cell and the ECM.

4.2. Continuous cell migration is driven by polymerization- and contraction/disassembly-induced flow of actin networks

Our simulations show that the continuous front polymerization and rear contraction of actin–myosin network create a steady retrograde flow of the network inside the cell. When coupled to the ECM through either adhesion molecules or steric effects, this flow generates traction forces to move the cell through the ECM. A similar conclusion was previously reached in [19]. Such traction force is balanced by resisting forces applied by the ECM to the cell front as well as the adhesion and friction forces on the side of the cell. This polymerization- and contractility-mediated flow of actin network has been shown to be stable at high Péclet number (stress-caused advection is stronger than diffusion of myosin) and generate traction forces against a 3D ECM [19]. This mechanism is continuous in time and does not require the assumption of periodic protrusion and contraction [17].

To see how the flow of actin network influences the speed of different migration modes, we simulated the migration of cells in all six modes at different v_g and v_s (figure 4). Since v_g and v_s are correlated with the polymerization and contraction rate, respectively, increasing both is expected to lead to an increased migration speed. Indeed, this is the case (figure 4). Note that v_g in our model is not the polymerization rate of actin, rather, v_g represents effective rate of actin network expansion.

By fixing $v_s = 0.01\ \mu\mathrm{m\,s^{-1}}$ and increasing v_g from 0.001 to 0.01 $\mu\mathrm{m\ s^{-1}}$, we find that the simulated v_{cell} increases by a factor of 1–4 for all migration modes (figure 4*a*). This suggests that cell speed is sensitive to the rate of actin polymerization

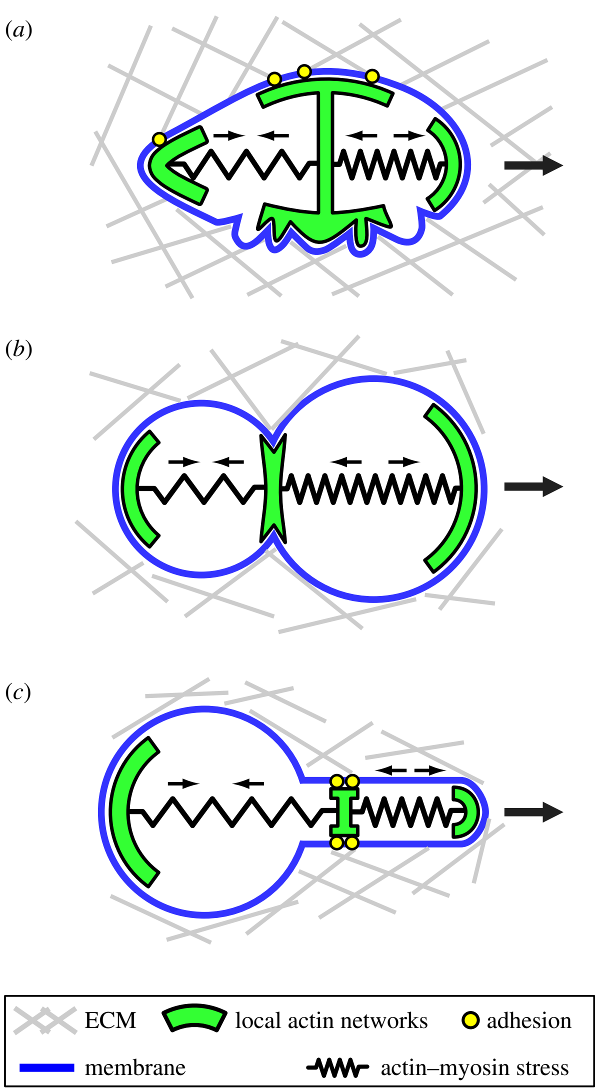

Figure 3. Proposed mechanics of cell migration in 3D ECM in five different modes. Actin–myosin network is roughly divided into three dynamic regions: protrusive (right), anchoring/traction (middle) and contraction (left). At the front of the cell, actin polymerization generates compressive stress (divergent thin black arrows) to push the cell front away from the anchoring/traction region in the middle. At the rear of the cell, actin disassembly and myosin-induced contraction generates contractive stress (convergent thin black arrows) to pull the cell body towards the anchoring/traction region in the middle. The continuous motion of cell in the direction indicated by the thick black arrow is achieved through actin network flow and effective treadmilling. (*a*) Mesenchymal (top membrane surface) or chimneying (bottom membrane surface) modes. (*b*) Amoeboid and blebbing modes (adhesions not shown). (*c*) Finger-like protruding mode.

when myosin-induced contraction is faster than actin growth. As v_g increases further from 0.01 to 0.1 μm s^{-1}, v_{cell} increases by a few tens of per cent for both blebbing and chimneying modes, but remains roughly unchanged for the other modes. The reason is that both blebbing and chimneying modes rely on the steric interactions between the cell and the ECM. Increasing polymerization rate will make the cell expand more efficiently into the pores of the ECM and thus increases the traction. On the other hand, the speed of adhesion-dependent migration relies on the flow rate of actin networks, which depends on both the polymerization and contraction rates of actin. For $v_g > v_s$, the actin flow rate is determined by the slower rate v_s. Therefore, v_{cell} becomes insensitive to v_g for $v_g > v_s$.

Table 3. Factors that influence migration modes.

	with proteolysis	without proteolysis
with adhesion	mesenchymal/rear-squeezing	amoeboid/finger-like
without adhesion	chimneying	amoeboid

By fixing $v_g = 0.01\ \mu\text{m s}^{-1}$ and increasing v_s, we find that v_{cell} increases by a factor of 2–13 for finger-like, mesenchymal and rear-squeezing modes but is roughly unaffected for amoeboid, blebbing and chimneying modes (figure 4*b*). This is because cells moving with the first three modes depend on myosin-induced contraction of actin networks while cells moving with the last three modes rely on the expansion of the cortex into the pores of the ECM. For cells migrating in the first three modes, there is a sharp increase in v_{cell} as v_s increases from 0.001 μm s^{-1} to 0.01 μm s^{-1}. Such increase is much slower as v_s increases further to 0.1 μm s^{-1}. This is due to the fact that efficient flow of actin networks depends on both the polymerization at the front and contraction at the rear. For cells moving in the last three modes, v_{cell} does not drop to 0 as v_s approaches 0 (figure 4*b*). This is because the continuous flow of actin can be maintained by front polymerization and rear disassembly even in the absence of myosin-induced contraction.

4.3. Migration speed depends on the lifetime of cell–extracellular matrix adhesion

To see how the lifetime of adhesions affects the migration speed, we varied k_d for four adhesion-dependent migration modes: amoeboid, finger-like, mesenchymal and rear-squeezing modes. We find that cells in these modes generally move more slowly as k_d increases from 0.01 to 1 s^{-1} (figure 5). An intuitive explanation is that transient adhesions facilitate cell migration by supporting higher traction forces on the side of the cell. Therefore, a high k_d will lead to a decreased traction force, and thus slow down the migration speed. On the other hand, a low k_d will increase the dragging force at the rear of the cell, which also slows down the migration speed. The combination of these two opposing effects leads to an optimal k_d where v_{cell} reaches maximum. This effect can be seen from our simulations in both mesenchymal and rear-squeezing modes (figure 5).

In addition to the self-detachment of adhesions, actin disassembly also releases the adhesions between the cell and ECM. As a result, the k_d-dependent dragging effect can be attenuated at $k_d < k_{dis} = 0.004\,\text{s}^{-1}$, leading to an increased migration speed at low k_d. Our simulations show that v_{cell} in both the amoeboid and finger-like modes plateaus as k_d decreases from 0.01 to 0.001 s^{-1} (figure 5), consistent with the idea that disassembly of actin takes into effect.

4.4. Migration speed depends on the mesh size

We examined how the mesh size of the ECM influences the speed of cells in different migration modes. We find that for all migration modes there exists an optimal ξ_{ECM} at

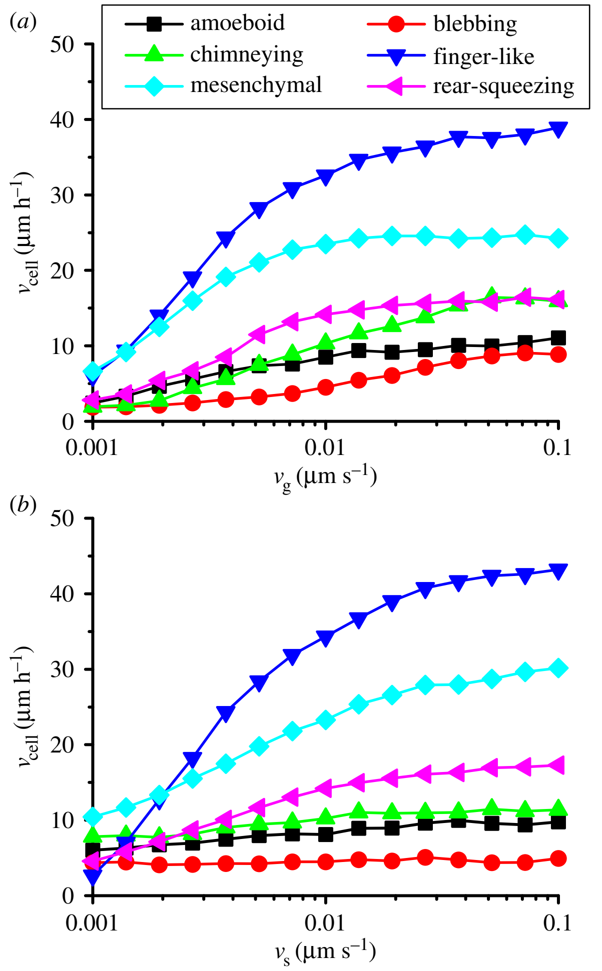

Figure 4. Cell speed as a function of (*a*) v_g and (*b*) v_s for all six migration modes.

which v_{cell} reaches the maximum (figure 6). Cells moving in amoeboid or blebbing mode reach their maximal speed when $\xi_{\mathrm{ECM}} \approx 13\,\mu\mathrm{m}$, which is right between the diameter of the nucleus (10 μm) and the diameter of the cell (16 μm). The reason is that cells moving in these two modes rely on the formation of pseudopodia into the pores of the ECM. A small ξ_{ECM} will hinder both the formation of pseudopodia into ECM pores and the translocation of nuclei into the pores, while a large ξ_{ECM} will cause inefficient generation of traction forces (figure 3*b*).

Cells moving in chimneying mode move mostly efficiently at $\xi_{\mathrm{ECM}} \approx 4\,\mu\mathrm{m}$, which is comparable to the largest mesh size of the actin network $l_{\max} = 4\,\mu\mathrm{m}$ in the simulations. The mesh size of our simulated actin–myosin network probably corresponds to the length scale of density variation in the actual networks, which correlates with the surface roughness of the cells. Since cells moving in this mode are driven by the steric interactions with the ECM, they will gain maximal traction and speed only if the size of their surface undulation is comparable with ξ_{ECM}.

For cells moving in mesenchymal or rear-squeezing mode, the fastest speed is achieved at $\xi_{\mathrm{ECM}} < 2\,\mu\mathrm{m}$. This is because a denser ECM allows for a higher probability of forming cell–ECM adhesions and thus a higher traction force. On the other hand, the drag force increases with the number of adhesions but is limited by the disassembly of actin networks. As a result, cells move faster in ECMs with smaller ξ_{ECM}.

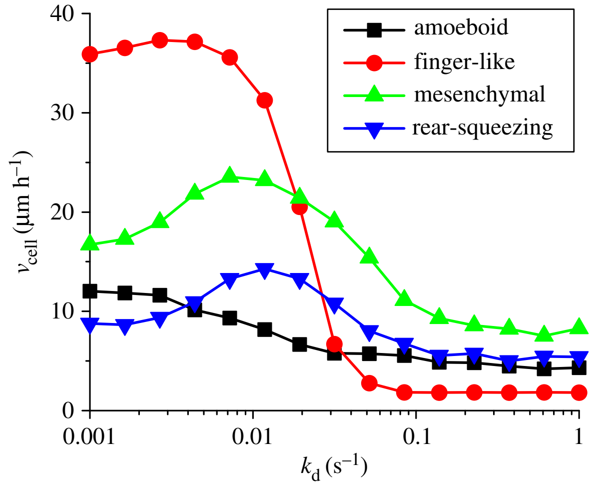

Figure 5. Cell speed dependence on the adhesion detachment rate.

For cells moving in finger-like mode, v_{cell} reaches maximum at $\xi_{\mathrm{ECM}} \approx 3\,\mu\mathrm{m}$. Similar to the mesenchymal and rear-squeezing mode, a higher traction force is obtained in a denser ECM due to increased chance of forming adhesion sites. But the resisting force, which is mainly from the steric effects between the bulging cell body and the ECM, also increase when the density of ECM increases. These two opposing effects lead to a maximal speed at ξ_{ECM} that is comparable with the width of the finger-like protrusion, which is set to be 2 μm in our simulations.

These results provoke thoughts about relevance of the nuclear size for different migration modes. Assuming that the overall cell size, excluding long protrusions, is of the same order of magnitude as that of the nucleus, amoeboid and blebbing mode would be optimal if ξ_{ECM} is of the same order of magnitude as the nuclear size. In all other modes, dragging the nucleus through ECM limits the locomotion, and so the smaller the nucleus, the better for the cell speed. Not surprisingly, active deformations of the nucleus (rigidity of the nucleus in the model is one of its major limitations) contribute crucially to a number of experimentally observed motility mechanisms. Lastly, in the rear-squeezing mode, the nucleus is not only the drag but also a 'ram' used by the cell instead of cytoskeleton-based protrusion.

4.5. Migration speed depends on the extracellular matrix stiffness

By varying the spring constant $k_{s,\mathrm{ECM}}$ of the ECM links, we are able to alter the Young's modulus of the ECM through $Y_{\mathrm{ECM}} = k_s/\xi_{\mathrm{ECM}}$ without changing the geometric structure of the ECM. The simulated v_{cell} as a function of Y_{ECM} with parameter values shown in table 2 is shown in figure 7.

For the range of Y_{ECM} between 1 Pa and 1000 Pa that we studied, the speed of finger-like migration shows a biphasic dependence and is very sensitive to Y_{ECM}: v_{cell} reaches a maximum value of about $34\,\mu\mathrm{m\,s}^{-1}$ at $Y_{\mathrm{ECM}} \approx 12\,\mathrm{Pa}$ and reduces by a factor of more than 5 as Y_{ECM} approaches either extreme values. For other migration modes, v_{cell} becomes less sensitive to Y_{ECM} with the maximum-to-minimum ratio of v_{cell} being approximately 2. In all migration modes except for finger-like mode, v_{cell} is

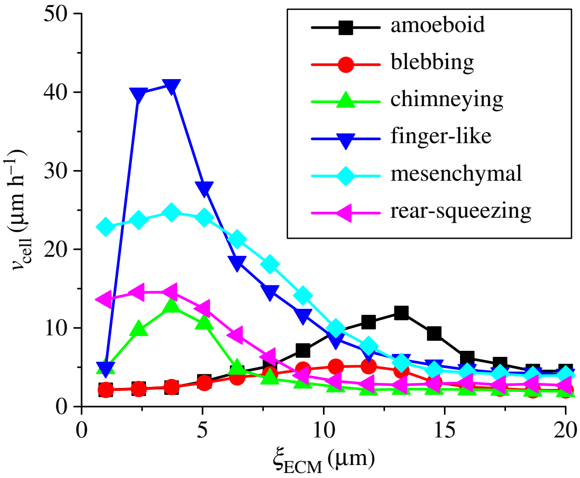

Figure 6. Cell speed dependence on the ECM mesh size.

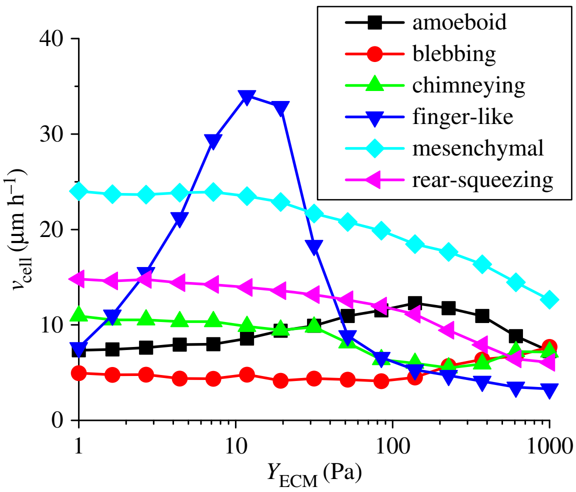

Figure 7. Cell speed dependence on the ECM Young's modulus.

insensitive to Y_{ECM} in the range of $Y_{\text{ECM}} = 1\text{–}10$ Pa but shows different trends as Y_{ECM} further increases to 1000 Pa: v_{cell} in amoeboid mode shows a weak biphasic dependence on Y_{ECM} with its maximal value at $Y_{\text{ECM}} = 120$ Pa; v_{cell} in chimneying mode has an opposite biphasic dependence on Y_{ECM} with its minimal value at $Y_{\text{ECM}} \approx 200$ Pa; v_{cell} increases monotonically in blebbing mode but decreases monotonically in both mesenchymal and rear-squeezing modes.

We explain that Y_{ECM} influences v_{cell} with the following arguments. A stiffer ECM will yield less when deformed by cells and thus better preserve its local structure. As a result, cells can exert stronger traction forces through steric interactions with the ECM and move faster. For finger-like mode where adhesion in the thin protrusion is critical for the generation of traction forces, a stiffer ECM will allow each adhesion site to exert a stronger traction force during its lifetime and thus make the cell move faster. On the other hand, the better preserved local structure of the ECM will produce a higher resistance force to the front of cells if local proteolytic activity is low, leading to a slower speed. In addition, the local structure of stiffer ECM will tend to divert the direction of cell migration, leading to a less persistent cell migration and thus a slower average speed. For cells moving in amoeboid or blebbing mode, the pores of a stiffer ECM is less likely to expand and will thus make the cell nucleus less likely to move through, which will also lead to a reduced speed of cell migration.

With the above effects, v_{cell} in different modes will have different dependencies on Y_{ECM}. For example, at low Y_{ECM}, cells in finger-like mode cannot produce strong traction forces and will move slowly; at high Y_{ECM}, these cells will experience high opposing forces at the front and will also move slowly; only at intermediate Y_{ECM} these cells can achieve optimal migration speed.

4.6. Phase diagram for migration modes

Since v_{cell} is not very sensitive to Y_{ECM}, we focus on how proteolytic activity, ξ_{ECM} and k_{d} affect v_{cell} and the migration modes. We simulate migration of cells with an initial radius of $R_{\text{cell}} = 8\,\mu\text{m}$ inside an ECM of $Y_{\text{ECM}} = 10$ Pa. By varying both ξ_{ECM} and k_{d}, we obtain contour plots of v_{cell} with and without proteolytic activity (figure 8).

We visually identified the migration modes for different combinations of ξ_{ECM} and k_{d}, and constructed a phase diagram of migration modes on top of the contour plots of v_{cell} (figure 8). Because we do not include the initial long protrusions of cells in this simulation, the finger-like mode is identified when cells form a single, long protrusion along the direction of migration. Other than finger-like mode, cells without proteolytic activity can be either amoeboid or blebbing type. They are differentiated by the number of adhesion sites: cells with an average of more than two adhesions are defined as amoeboid type while others are defined as blebbing type. Since we do not include the biased nucleation of actin in this simulation, the rear-squeezing mode is not included in the phase diagram.

For cells without proteolytic activity (figure 8*a*), we find two local maxima: one is at $\xi_{\text{ECM}} \approx 2\,\mu\text{m}$ and $k_{\text{d}} \approx 0.001\,\text{s}^{-1}$, the other is at $\xi_{\text{ECM}} \approx 12\,\mu\text{m}$ and $k_{\text{d}} \approx 0.001\,\text{s}^{-1}$. By comparing the migration modes, we find that the first maximum corresponds to a finger-like migration, and that the second maximum corresponds to an amoeboid migration. Cells in amoeboid mode can reach a maximum speed of $v_{\text{cell}} \approx 15\,\mu\text{m}\,\text{h}^{-1}$ while those in finger-like mode have a maximum speed of approximately $10\,\mu\text{m}\,\text{h}^{-1}$. The speed of finger-like migration in this simulation is much slower than the one simulated previously (figure 6) because these cells do not have the prescribed protrusion where adhesions and actin contraction are highly active. From figure 8*a*, we find that finger-like mode occurs at $\xi_{\text{ECM}} < 5\,\mu\text{m}$ and $k_{\text{d}} < 0.005\,\text{s}^{-1}$. Amoeboid mode occurs at $5\,\mu\text{m} < \xi_{\text{ECM}} < 20\,\mu\text{m}$ and $k_{\text{d}} < 0.06\,\text{s}^{-1}$. Blebbing mode happens at $5\,\mu\text{m} < \xi_{\text{ECM}} < 14\,\mu\text{m}$ and $k_{\text{d}} > 0.06\,\text{s}^{-1}$. The boundary between amoeboid and finger-like modes is roughly along $\xi_{\text{ECM}} = 5\,\mu\text{m}$, which is likely to be determined by the available area of protruding pseudopodia.

For cells with proteolytic activity (figure 8*b*), we find that the most effective cell migration happens at $\xi_{\text{ECM}} < 12\,\mu\text{m}$. There exists a single local maximum at $\xi_{\text{ECM}} \approx 5\,\mu\text{m}$ and $k_{\text{d}} \approx 0.005\,\text{s}^{-1}$ where cells move in mesenchymal mode. For $\xi_{\text{ECM}} < 8\,\mu\text{m}$ and $k_{\text{d}} > 0.1\,\text{s}^{-1}$, chimneying mode starts to emerge but with a much slower speed. Wolf *et al.* [11] found that inhibition of proteolytic activity on mesenchymal HT-1080/MT1 cells in 3D collagen matrix switches the cell into amoeboid mode but does not change the migration

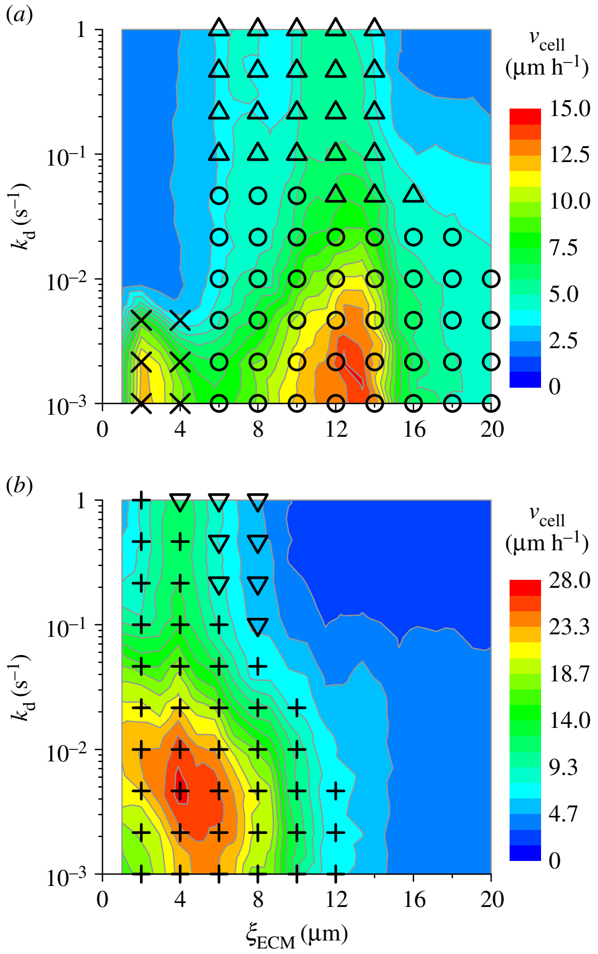

Figure 8. Simulated speed and migration modes for cells without proteolysis (*a*) and with proteolysis (*b*). Symbols indicate simulated modes of migration. Circles, amoeboid mode; up-triangles, blebbing mode; crosses, finger-like mode; pluses, mesenchymal mode; down-triangles, chimneying mode.

speed. This finding corresponds to $\xi_{ECM} = 14\,\mu m$ and $k_d < 0.01\,s^{-1}$ in our simulation where switching off proteolytic activity changes the migration mode from mesenchymal to amoeboid but v_{cell} remains about the same.

5. Discussion

Our simulations suggest that observed modes of 3D cell migration can be explained by a single model which has three main components: protrusion, contraction and adhesion. We find that we can reproduce five modes of motility if we include or exclude proteolysis of ECM, and vary adhesion/detachment rate, and spatial distributions of protrusion, contraction and adhesion. Specifically, mesenchymal mode requires strong proteolytic activity and low-adhesion detachment rate. Chimneying mode works in the absence of adhesions, but requires proteolytic activity. Amoeboid and blebbing modes persist with inhibited proteolysis and the low-adhesion level. Finger-like protrusion mode requires actin expansion at the tip of the protrusion, strong adhesions along the protrusion, strong contraction at the base of protrusion and an ECM that can be easily ruptured. In this mode, proteolysis is dispensable. Lastly, in the rear-squeezing mode, actin network has to be concentrated behind the nucleus, so that the contraction of the actin network can generate a squeezing force on the nucleus to push the cell forward.

We further find that the mode of the cell motility could evolve without changing parameters or spatial distributions in response to the ECM and adhesion properties: without proteolysis, cells choose the finger-like protrusion mode in the dense ECM, and amoeboid mode in ECM with larger mesh size. The amoeboid mode becomes blebbing mode in the absence of adhesions. With proteolysis, cells move in chimneying mode in low-density, low-adhesion ECM and in mesenchymal mode in dense adhesive ECM.

The model makes a number of interesting quantitative predictions: the finger-like protrusion mode is sensitive to the ECM elasticity; cell speed peaks at an intermediate elasticity. Speed in other modes is not very sensitive to the ECM elasticity. Cell speed in the majority of modes is sensitive to the ECM mesh size; there is an optimal ECM density, specific for each mode. There is an optimal adhesion strength maximizing speed in mesenchymal and rear-squeezing modes, while the speed is a decreasing function of the adhesion strength in amoeboid and finger-like protrusion modes.

One general conclusion is that cells can sometime dispense either the front protrusion, or the rear contraction, or adhesions, but the rearward flow of the cortical actin network is always important for migration in 3D. Without rear contraction, the flow of the actin network is weak, which slows down the cell migration speed but does not stop the motion. Without adhesions, cells can move via steric interactions with the ECM by forming small protrusions to 'grab' on the structures of the ECM. Thus, the retrograde flow of the actin network and its mechanical coupling to ECM is a versatile driving mechanism for cell migration in 3D. In addition, proteolysis is important for efficient mesenchymal migration in a dense ECM. One interesting result is that the combination of parameters yielding minimal migration speed lies roughly along the diagonal line from low proteolysis + high k_d + small ξ_{ECM} to high proteolysis + low k_d + large ξ_{ECM}.

Our model is conceptual, rather than comprehensive: it does not consider the effect of membrane blebbing. ECM in the model is represented by interconnected nodes, and the cell interacts with the ECM only through these nodes, not with the ECM fibres. Importantly, the model does not include random competing protrusions. Besides, the simulations would have to be redone in the asymmetric 3D case, which presents a significant computational challenge. One of the consequences of these simplifications is that the predicted 'snail trails' in figure 2 indicating a footprint of cell passage do not correspond well to experimental observations. In addition, the prediction of non-altered tension in the remodelled ECM adjacent to the passage of the cell does not agree well with observations. Future simulations of the realistic nonlinear, mechanosensing, mechanochemical, history-dependent and viscoelastic properties of the actin–myosin and ECM networks, and nucleus will be required.

We should note that the parameters with which we describe the physical properties of ECM, such as ξ_{ECM} and Y_{ECM}, are typically interdependent. For example, increasing the density of ECM can increase Y_{ECM} but will decrease ξ_{ECM}; Y_{ECM} can be changed without affecting ξ_{ECM} by using a different ECM material, but it is likely to influence the adhesion dynamics. Studying the relation between these factors is beyond the scope of current study. In our model, the detachment rate of cell–ECM adhesions is simplified to be a constant k_d. But in reality, such detachment rate may depend on the stress or strain in a nonlinear fashion. Such dependence will impact our $v_{cell} - k_d$ relation in complicated ways. A detailed study of how different dependence of k_d on the force or strain will be included in the future to improve our model. Last, but not least, continuous modelling of the 3D cell migration [28–31] has to be explored in parallel with discrete computational models, such as ours.

There is a great recent surge in experimental research in 3D cell migration [15,32–34], and, fittingly, modelling studies started to address theoretical questions about the mechanics of cell migration in ECM [20,35–38]. Very recently, modelling and experiment on the 3D migration started to merge [39–41]. Our study, hopefully, will contribute to understanding of the general mechanical principles of the 3D motility.

Competing interests. We declare we have no competing interests.
Funding. This work is supported by NIH grant no. GM-068952 to A.M.

References

1. Bray D. 2001 *Cell movements: from molecules to motility*, 2nd edn. New York, NY: Garland Publisher.
2. Svitkina TM, Verkhovsky AB, McQuade KM, Borisy GG. 1997 Analysis of the actin-myosin II system in fish epidermal keratocytes: mechanism of cell body translocation. *J. Cell Biol.* **139**, 397–415. (doi:10.1083/jcb.139.2.397)
3. Ji L, Lim J, Danuser G. 2008 Fluctuations of intracellular forces during cell protrusion. *Nat. Cell. Biol.* **10**, 1393–1400. (doi:10.1038/ncb1797)
4. Gardel ML, Schneider IC, Aratyn-Schaus Y, Waterman CM. 2010 Mechanical integration of actin and adhesion dynamics in cell migration. *Annu. Rev. Cell Dev. Biol.* **26**, 315–333. (doi:10.1146/annurev.cellbio.011209.122036)
5. Gardel ML, Sabass B, Ji L, Danuser G, Schwarz US, Waterman CM. 2008 Traction stress in focal adhesions correlates biphasically with actin retrograde flow speed. *J. Cell Biol.* **183**, 999–1005. (doi:10.1083/jcb.200810060)
6. Lammermann T *et al.* 2008 Rapid leukocyte migration by integrin-independent flowing and squeezing. *Nature* **453**, 51–55. (doi:10.1038/nature06887)
7. Petrie RJ, Gavara N, Chadwick RS, Yamada KM. 2012 Nonpolarized signaling reveals two distinct modes of 3D cell migration. *J. Cell Biol.* **197**, 439–455. (doi:10.1083/jcb.201201124)
8. Vanni S, Lagerholm BC, Otey C, Taylor DL, Lanni F. 2003 Internet-based image analysis quantifies contractile behavior of individual fibroblasts inside model tissue. *Biophys. J.* **84**, 2715–2727. (doi:10.1016/S0006-3495(03)75077-2)
9. Legant WR, Miller JS, Blakely BL, Cohen DM, Genin GM, Chen CS. 2010 Measurement of mechanical tractions exerted by cells in three-dimensional matrices. *Nat. Methods* **7**, 969–971. (doi:10.1038/nmeth.1531)
10. Shih W, Yamada S. 2010 Myosin IIA dependent retrograde flow drives 3D cell migration. *Biophys. J* **98**, L29–L31. (doi:10.1016/j.bpj.2010.02.028)
11. Wolf K, Mazo I, Leung H, Engelke K, von Andrian UH, Deryugina EI, Strongin AY, Brocker EB, Friedl P. 2003 Compensation mechanism in tumor cell migration: mesenchymal-amoeboid transition after blocking of pericellular proteolysis. *J. Cell Biol.* **160**, 267–277. (doi:10.1083/jcb.200209006)
12. Friedl P, Wolf K. 2009 Proteolytic interstitial cell migration: a five-step process. *Cancer Metastasis Rev.* **28**, 129–135. (doi:10.1007/s10555-008-9174-3)
13. Sanz-Moreno V, Gadea G, Ahn J, Paterson H, Marra P, Pinner S, Sahai E, Marshall CJ. 2008 Rac activation and inactivation control plasticity of tumor cell movement. *Cell* **135**, 510–523. (doi:10.1016/j.cell.2008.09.043)
14. Zaman MH, Trapani LM, Sieminski AL, Mackellar D, Gong H, Kamm RD, Wells A, Lauffenburger DA, Matsudaira P. 2006 Migration of tumor cells in 3D matrices is governed by matrix stiffness along with cell-matrix adhesion and proteolysis. *Proc. Natl Acad. Sci. USA* **103**, 10 889–10 894. (doi:10.1073/pnas.0604460103)
15. Doyle AD, Wang FW, Matsumoto K, Yamada KM. 2009 One-dimensional topography underlies three-dimensional fibrillar cell migration. *J. Cell Biol.* **184**, 481–490. (doi:10.1083/jcb.200810041)
16. Guetta-Terrier C *et al.* 2015 Protrusive waves guide 3D cell migration along nanofibers. *J. Cell Biol.* **211**, 683–701. (doi:10.1083/jcb.201501106)
17. Zaman MH, Kamm RD, Matsudaira P, Lauffenburger DA. 2005 Computational model for cell migration in three-dimensional matrices. *Biophys. J.* **89**, 1389–1397. (doi:10.1529/biophysj.105.060723)
18. Borau C, Kamm RD, Garcia-Aznar JM. 2011 Mechano-sensing and cell migration: a 3D model approach. *Phys. Biol.* **8**, 066008. (doi:10.1088/1478-3975/8/6/066008)
19. Hawkins RJ, Poincloux R, Benichou O, Piel M, Chavrier P, Voituriez R. 2011 Spontaneous contractility-mediated cortical flow generates cell migration in three-dimensional environments. *Biophys. J.* **101**, 1041–1045. (doi:10.1016/j.bpj.2011.07.038)
20. Sakamoto Y, Prudhomme S, Zaman MH. 2014 Modeling of adhesion, protrusion, and contraction coordination for cell migration simulations. *J. Math. Biol.* **68**, 267–302. (doi:10.1007/s00285-012-0634-6)
21. Tozluoglu M, Tournier AL, Jenkins RP, Hooper S, Bates PA, Sahai E. 2013 Matrix geometry determines optimal cancer cell migration strategy and modulates response to interventions. *Nat. Cell Biol.* **15**, 751–762. (doi:10.1038/ncb2775)
22. Zhu J, Mogilner A. 2012 Mesoscopic model of actin-based propulsion. *PLoS Comput Biol* **8**, e1002764. (doi:10.1371/journal.pcbi.1002764)
23. John K, Caillerie D, Peyla P, Raoult A, Misbah C. 2013 Nonlinear elasticity of cross-linked networks. *Phys. Rev. E Stat. Nonlin. Soft Matter Phys.* **87**, 042721. (doi:10.1103/PhysRevE.87.042721)
24. Bottino D, Mogilner A, Roberts T, Stewart M, Oster G. 2002 How nematode sperm crawl. *J. Cell Sci.* **115**, 367–384.
25. Hawkins RJ, Piel M, Faure-Andre G, Lennon-Dumenil AM, Joanny JF, Prost J, Voituriez R. 2009 Pushing off the walls: a mechanism of cell motility in confinement. *Phys. Rev. Lett.* **102**, 058103. (doi:10.1103/PhysRevLett.102.058103)
26. Bergert M, Chandradoss SD, Desai RA, Paluch E. 2012 Cell mechanics control rapid transitions between blebs and lamellipodia during migration. *Proc. Natl Acad. Sci. USA* **109**, 14 434–14 439. (doi:10.1073/pnas.1207968109)
27. Strychalski W, Guy RD. 2013 A computational model of bleb formation. *Math. Med. Biol.* **30**, 115–130. (doi:10.1093/imammb/dqr030)
28. Herant M, Dembo M. 2010 Form and function in cell motility: from fibroblasts to keratocytes. *Biophys. J.* **98**, 1408–1417. (doi:10.1016/j.bpj.2009.12.4303)
29. George UZ, Stephanou A, Madzvamuse A. 2013 Mathematical modelling and numerical simulations of actin dynamics in the eukaryotic cell. *J. Math. Biol.* **66**, 547–593. (doi:10.1007/s00285-012-0521-1)
30. Allena R, Aubry D. 2012 'Run-and-tumble' or 'look-and-run'? A mechanical model to explore the behavior of a migrating amoeboid cell. *J. Theor. Biol.* **306**, 15–31. (doi:10.1016/j.jtbi.2012.03.041)
31. Stolarska MA, Kim Y, Othmer HG. 2009 Multi-scale models of cell and tissue dynamics. *Phil. Trans. R. Soc. A* **367**, 3525–3553. (doi:10.1098/rsta.2009.0095)
32. Even-Ram S, Yamada KM. 2005 Cell migration in 3D matrix. *Curr. Opin. Cell Biol.* **17**, 524–532. (doi:10.1016/j.ceb.2005.08.015)
33. Martins GG, Kolega J. 2006 Endothelial cell protrusion and migration in three-dimensional collagen matrices. *Cell Motil. Cytoskelet.* **63**, 101–115. (doi:10.1002/cm.20104)
34. Petrie RJ, Yamada KM. 2012 At the leading edge of three-dimensional cell migration. *J. Cell Sci.* **125**, 5917–5926. (doi:10.1242/jcs.093732)

35. Rangarajan R, Zaman MH. 2008 Modeling cell migration in 3D: status and challenges. *Cell Adhesion Migration* **2**, 106–109. (doi:10.4161/cam.2.2.6211)
36. Tozluoglu M, Mao Y, Bates PA, Sahai E. 2015 Cost-benefit analysis of the mechanisms that enable migrating cells to sustain motility upon changes in matrix environments. *J. R. Soc. Interface* **12**, 20141355. (doi:10.1098/rsif.2014.1355)
37. Madsen CD, Hooper S, Tozluoglu M, Bruckbauer A, Fletcher G, Erler JT, Bates PA, Thompson B, Sahai E. 2015 STRIPAK components determine mode of cancer cell migration and metastasis. *Nat. Cell Biol.* **17**, 68–80. (doi:10.1038/ncb3083)
38. Borau C, Polacheck WJ, Kamm RD, Garcia-Aznar JM. 2014 Probabilistic voxel-Fe model for single cell motility in 3D. *In Silico Cell Tissue Sci.* **1**, 2. (doi:10.1186/2196-050X-1-2)
39. Liu YJ, Le Berre M, Lautenschlaeger F, Maiuri P, Callan-Jones A, Heuze M, Takaki T, Voituriez R, Piel M. 2015 Confinement and low adhesion induce fast amoeboid migration of slow mesenchymal cells. *Cell* **160**, 659–672. (doi:10.1016/j.cell.2015.01.007)
40. Ruprecht V *et al.* 2015 Cortical contractility triggers a stochastic switch to fast amoeboid cell motility. *Cell* **160**, 673–685. (doi:10.1016/j.cell.2015.01.008)
41. Bergert M, Erzberger A, Desai RA, Aspalter IM, Oates AC, Charras G, Salbreux G, Paluch EK. 2015 Force transmission during adhesion-independent migration. *Nat. Cell Biol.* **17**, 524–529. (doi:10.1038/ncb3134)